

Analytic description and optimization of magneto-optical Kerr setups with photoelastic modulation

Cite as: Rev. Sci. Instrum. **93**, 073001 (2022); <https://doi.org/10.1063/5.0088610>

Submitted: 18 February 2022 • Accepted: 08 June 2022 • Published Online: 06 July 2022

 Katherine Légaré,  Valentin Chardonnet,  Ivette Bermúdez Macias, et al.



View Online



Export Citation



CrossMark

ARTICLES YOU MAY BE INTERESTED IN

[Progress in in situ x-ray imaging of welding process](#)

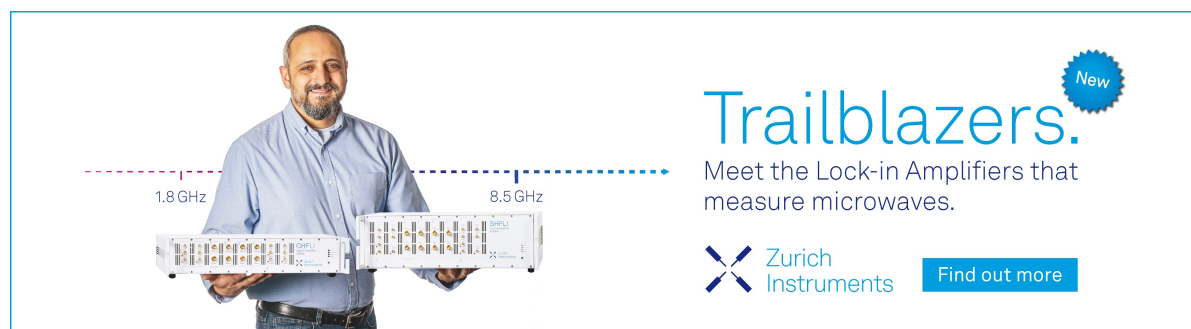
Review of Scientific Instruments **93**, 071501 (2022); <https://doi.org/10.1063/5.0074042>


[Liquid-cooled modular gas cell system for high-order harmonic generation using high average power laser systems](#)

Review of Scientific Instruments **93**, 073002 (2022); <https://doi.org/10.1063/5.0097788>


[Calibration of micro-channel plate detector in a Thomson spectrometer for protons and carbon ions with energies below 1 MeV](#)

Review of Scientific Instruments **93**, 073301 (2022); <https://doi.org/10.1063/5.0086747>



Trailblazers. 

Meet the Lock-in Amplifiers that measure microwaves.

 Zurich Instruments [Find out more](#)

Analytic description and optimization of magneto-optical Kerr setups with photoelastic modulation

Cite as: Rev. Sci. Instrum. 93, 073001 (2022); doi: 10.1063/5.0088610

Submitted: 18 February 2022 • Accepted: 8 June 2022 •

Published Online: 6 July 2022



Katherine Légaré,^{1,a)} Valentin Chardonnet,² Ivette Bermúdez Macias,³ Marcel Hennes,² Renaud Delaunay,² Philippe Lassonde,¹ François Légaré,¹ Guillaume Lambert,⁴ Emmanuelle Jal,² and Boris Vodungbo^{2,a)}

AFFILIATIONS

¹ Institut National de la Recherche Scientifique, Centre Énergie Matériaux Télécommunications (INRS-EMT), 1650 Boulevard Lionel-Boulet, Varennes, Québec J3X1P7, Canada

² Sorbonne Université, CNRS, Laboratoire de Chimie Physique-Matière et Rayonnement, LCPMR, 75005 Paris, France

³ Deutsches Elektronen-Synchrotron-DESY, Notkestraße 85, 22607 Hamburg, Germany

⁴ Laboratoire d'Optique Appliquée, ENSTA Paris, CNRS, École Polytechnique, Institut Polytechnique de Paris, 828 Boulevard des Maréchaux, Palaiseau Cedex 91762, France

^{a)} Authors to whom correspondence should be addressed: katherine.legare@inrs.ca and boris.vodungbo@sorbonne-universite.fr

ABSTRACT

Instruments based on the magneto-optical Kerr effect are routinely used to probe surface magnetic properties. These tools rely on the characterization of the polarization state of reflected light from the sample to collect information on its magnetization. Here, we present a theoretical optimization of common setups based on the magneto-optical Kerr effect. A detection scheme based on a simple analyzer and photodetector and one made from a polarizing beam splitter and balanced photodetectors are considered. The effect of including a photoelastic modulator (PEM) and a lock-in amplifier to detect the signal at harmonics of the modulating frequency is studied. Jones formalism is used to derive general expressions that link the intensity of the measured signal to the magneto-optical Fresnel reflection coefficients for any orientation of the polarizing optical components. Optimal configurations are then defined as those that allow measuring the Kerr rotation and ellipticity while minimizing nonmagnetic contributions from the diagonal Fresnel coefficients in order to improve the signal-to-noise ratio (SNR). The expressions show that with the PEM, setups based on polarizing beam splitters inherently offer a twofold higher signal than commonly used analyzers, and the experimental results confirm that the SNR is improved by more than 150%. Furthermore, we find that while all proposed detection schemes measure Kerr effects, only those with polarizing beam splitters allow measuring the Kerr rotation directly when no modulator is included. This accommodates, for instance, time-resolved measurements at relatively low laser pulse repetition rates. Ultrafast demagnetization measurements are presented as an example of such applications.

Published under an exclusive license by AIP Publishing. <https://doi.org/10.1063/5.0088610>

I. INTRODUCTION

The magneto-optical Kerr effect (MOKE),¹ which describes the change in the polarization and intensity of light upon reflection on a magnetic medium, has proven a valuable tool to probe the magnetic properties of material surfaces and thin films. Due to the simplicity of implementation of the technique, its advantageous temporal and spatial resolution,² its high sensitivity down to the monolayer,³ and the possibility to resolve thin film layers in complex structures,^{4,5}

the MOKE has been widely used for characterizing magnetic samples. It has proven to be useful in many fields, including micro-magnetics,^{6,7} data recording technologies,⁸ and spintronics.⁹ This method has also been applied to track the magnetic dynamics of solid-state samples in the context of ultrafast time-resolved experiments.^{10,11}

Several different experimental setups have been proposed to detect Kerr effects. In many cases, the measured signal is merely related to the Kerr rotation of the polarization, which is commonly

assumed to be directly proportional to the magnetization.¹² However, in some contexts, a complete characterization of the final polarization is essential to gather an accurate understanding of the magnetic state of the system.^{13,14} In particular, in the ultrafast magnetism community, research is ongoing to untangle the magnetic dynamics from charge dynamics, which may also affect the signal when the electronic system is strongly out of equilibrium.^{15–17} In this prospect, studies have shown that both the Kerr rotation and the Kerr ellipticity must be retrieved in order to relate the measurement to the magnetization as each of these quantities alone offers incomplete information.^{18–20} This is not possible with every MOKE detection scheme. For example, in the simple case where the magnetic sample is placed between two crossed polarizers, the measured signal corresponds to the intensity that is transferred to the orthogonal polarization component through Kerr effects. In this case, the signal simultaneously originates from the rotation of the polarization and from variations in the ellipticity, and it is not possible to decouple these contributions. In the following, we show that amendments to this detection scheme allow for direct, independent measurements of these quantities.

In magnetic materials, the presence of magnetization induces optical anisotropy, which is expressed by a dielectric tensor with complex off-diagonal elements.²¹ Upon reflection of polarized light onto such materials, the interaction between the electromagnetic field and the electrons leads to changes in the polarization state, which can be described by a complex Fresnel reflection matrix with non-zero off-diagonal elements.^{22,23} Using Jones matrices as a mathematical tool to describe the evolution of the polarization of the beam through the optical components of the experimental setup, it is possible to relate the measured signal to these Fresnel coefficients. This approach aims not only to ensure the independent measurement of Kerr rotation and ellipticity, which can also be defined from the Fresnel coefficients, but also to identify configurations with an optimal signal-to-noise ratio (SNR) by minimizing the nonmagnetic background brought by the contribution of the diagonal components of the Fresnel matrix.

Here, Jones formalism is used to study two common MOKE setups. The first setup relies on a simple polarizer to analyze changes in the polarization of the reflected beam. The second setup includes a half-waveplate and a polarizing beam splitter to simultaneously detect and eventually subtract the two orthogonal polarization components. In both cases, we also study the effect of adding a photoelastic modulator (PEM) and a lock-in amplifier to the detection scheme. This block is often included to reduce noise but can be inconvenient to use in conjunction with a pulsed laser source with a low repetition rate. For each detection scheme, a general expression is derived, which describes the measured signal as a function of the Fresnel coefficients for all possible orientations of the polarizing optical elements. These expressions are then used to deduce optimal configurations in which the nonmagnetic contribution to the signal is canceled and configurations in which the signal is proportional to the Kerr rotation or ellipticity. Similar work, published by Polisetty *et al.*,²⁴ has previously shown that for a detection scheme based on a simple polarizer and including a PEM, one optimal configuration is achieved by rotating the transmission axis of the analyzer by 45° with respect to the incident polarization, which is perpendicular to the plane of incidence (*s*-polarization). Indeed, this configuration maximizes the magnetic signal when reading the first or second harmonic

of the modulating frequency. Here, we demonstrate from the more general equations that an equivalent configuration can be found for incident *p*-polarization (component lying in the plane of incidence). Furthermore, we establish that experimental setups based on a polarizing beam splitter offer a signal that is twice as large as setups based on analyzers and that the SNR scales accordingly. In addition, we find that when modulators and lock-in amplifiers are excluded, only the polarizing beam splitter setup allows for direct reading of the Kerr rotation and that it can also be adapted to measure the Kerr ellipticity. We show that this configuration is then suitable for pump-probe time-resolved experiments and that it can accommodate fast single-shot measurements. As an example, we apply it to the study of laser-induced ultrafast demagnetization in a Co/Pt multilayer sample. This article is organized into three parts: Sec. II describes the different detection schemes studied, Sec. III details how we used the Jones formalism to find the optimal MOKE configurations, and Sec. IV shows the experimental confirmation of our theoretical optimization for static and time-resolved measurements.

II. DESCRIPTION OF THE DETECTION SCHEMES

To detect changes in the polarization of a linearly polarized incident beam after reflection on the magnetic sample, some schemes rely on a simple polarizer followed by a photodetector.^{10,25–27} Others exploit polarizing beam splitters to separate the reflected polarization components and subtract them.^{28,29} Many experimental setups also include a modulator and a lock-in amplifier to improve the SNR,^{24,30,31} which is essential because Kerr effects are typically very small. The MOKE configurations studied in this work are presented in Fig. 1(a). First, the laser beam passes through a polarizer before being focused by a lens onto the sample. Then, the reflected beam is recollimated by a second lens and optionally goes through a PEM before its polarization is finally analyzed. The effect of the PEM is to introduce a periodic phase shift between the *s*- and *p*-polarization components of the beam. If the PEM is used, the collected signal is sent to a lock-in amplifier that only detects signals at harmonics of the modulating frequency, thereby reducing noise in the final measurement. In all configurations, the magnetic sample is placed in a magnetic field generated by an electromagnet so that a whole hysteresis curve can be measured.

The first MOKE setup studied in this work is the simple case where the polarization detection scheme consists of a mere analyzer followed by a photodetector. This configuration, used with the PEM and lock-in amplifier, will be termed the “modulator-analyzer setup” in the following [inset in Fig. 1(a)]. In the second version of the setup presented here, the analyzer is replaced by a half-waveplate and a polarization beam splitter (PBS). The single photodetector is replaced by two balanced photodetectors. This way, instead of one vector component of the signal’s electric field being measured while the other is completely removed by the analyzer, the signal is split into its two orthogonal polarization components and both of them are detected. The output of the balanced photodetectors corresponds to the amplified difference between the two signals, leading to a theoretical twofold increase in the measured intensity compared to the analyzer schemes. In the following, this setup configuration will be termed the “modulator-PBS setup” [Fig. 1(a)].

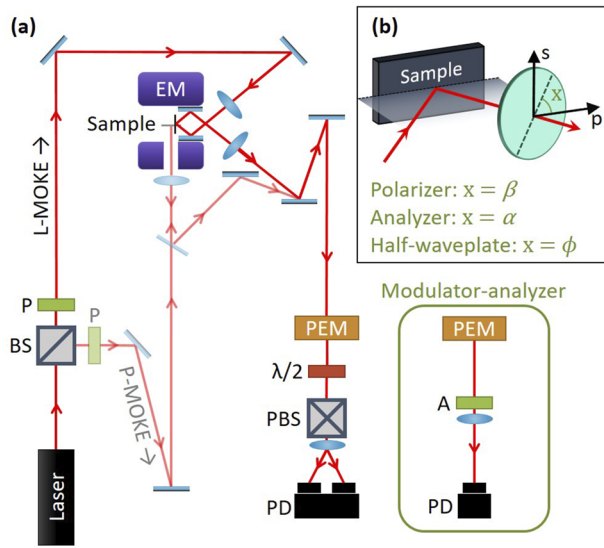


FIG. 1. (a) Sketch of the modulator-PBS MOKE setup. The equivalent modulator-analyzer detection scheme is shown in the inset. The bright path corresponds to a longitudinal MOKE setup, while the pale path corresponds to a polar MOKE setup. The components are the beam splitter (BS), polarizer (P), electro-magnet (EM), photoelastic modulator (PEM), half-waveplate ($\lambda/2$), analyzer (A), polarizing beam splitter (PBS), and photodetectors (PDs). The magnetic field MOKE is in the sample plane for the longitudinal MOKE and out-of-plane for the polar MOKE. (b) Definition of the orientation of the optical axis or transmission axis of each optical component with respect to the plane of incidence.

Conventionally, three different magneto-optical Kerr effects are identified, differing only in the relative orientation of the magnetization with respect to the plane of incidence and the surface of the sample. The polar, longitudinal, and transverse Kerr effects correspond to the cases in which the magnetization is perpendicular to the sample surface, parallel to the surface and to the plane of incidence, or parallel to the surface and perpendicular to the plane of incidence, respectively. It should be noted that this work pertains solely to the polar and longitudinal MOKE and that no conclusion has been drawn concerning the transverse Kerr effect, which yields variations in the reflected intensity rather than changes in the polarization state.

III. JONES FORMALISM

In Jones formalism, a polarization state is described by a two-element vector $E = \begin{bmatrix} E_p \\ E_s \end{bmatrix}$, where E_p and E_s represent the proportion of the electric field in p - and s -polarizations, respectively. Each optical component of the setup can be described by a two by two transformation matrix that modifies this polarization state. For the MOKE setups, the initial polarization after the first polarizer is represented by the vector $P = \begin{bmatrix} \cos \beta \\ \sin \beta \end{bmatrix}$. In the analyzer-based setups, the analyzer is a mere polarizer and is represented by the following matrix:

$$A = \begin{bmatrix} \cos^2 \alpha & \cos \alpha \sin \alpha \\ \cos \alpha \sin \alpha & \sin^2 \alpha \end{bmatrix}. \quad (1)$$

The matrix of the half-waveplate used in the PBS-based MOKE setups is

$$H = \begin{bmatrix} -i \cos(2\phi) & -i \sin(2\phi) \\ -i \sin(2\phi) & i \cos(2\phi) \end{bmatrix}. \quad (2)$$

The arguments β , α , and ϕ correspond to the angles between the optical axis or transmission axis of the component and the plane of incidence [Fig. 1(b)]. For simplicity, we consider that the PBS is set to split the s - and p -polarization components of the beam. Thus, the PBS is not represented by a matrix. Instead, the vector components of the final polarization state are considered independently to simulate the separation of the s - and p -polarizations. The sample is represented by the corresponding magneto-optical Fresnel reflection matrix²³ as follows:

$$S = \begin{bmatrix} \tilde{r}_{pp} & \tilde{r}_{ps} \\ \tilde{r}_{sp} & \tilde{r}_{ss} \end{bmatrix} = \begin{bmatrix} r_{pp} e^{i\delta_{pp}} & r_{ps} e^{i\delta_{ps}} \\ r_{sp} e^{i\delta_{sp}} & r_{ss} e^{i\delta_{ss}} \end{bmatrix}, \quad (3)$$

where \tilde{r}_{kl} is the ratio of the component of the reflected electric field polarized along the k axis and the component of the incident electric field polarized along the l axis. Each complex Fresnel coefficient can be separated into the amplitude of the reflectivity r_{kl} and its phase δ_{kl} . The magnetic information is contained in the off-diagonal elements. Indeed, if these elements were equal to zero, there would be no change in the polarization state upon reflection on the magnetic sample. Hence, the complex Kerr angles are defined as $\Theta_p = \frac{\tilde{r}_{sp}}{\tilde{r}_{pp}} = \frac{r_{sp}}{r_{pp}} e^{i(\delta_{sp} - \delta_{pp})}$ and $\Theta_s = \frac{\tilde{r}_{ps}}{\tilde{r}_{ss}} = \frac{r_{ps}}{r_{ss}} e^{i(\delta_{ps} - \delta_{ss})}$. The real part of the complex Kerr angle can be associated with the Kerr rotation $\theta_{s,p}$, while the imaginary part represents the Kerr ellipticity $\epsilon_{s,p}$,

$$\begin{aligned} \theta_s &= \frac{r_{ps}}{r_{ss}} \cos(\delta_{ps} - \delta_{ss}), \\ \theta_p &= \frac{r_{sp}}{r_{pp}} \cos(\delta_{sp} - \delta_{pp}), \\ \epsilon_s &= \frac{r_{ps}}{r_{ss}} \sin(\delta_{ps} - \delta_{ss}), \\ \epsilon_p &= \frac{r_{sp}}{r_{pp}} \sin(\delta_{sp} - \delta_{pp}). \end{aligned} \quad (4)$$

The following matrix expresses the retardation $\varphi = \varphi_0 \sin(\omega t)$ caused by the PEM:

$$O = \begin{bmatrix} e^{i\frac{\varphi}{2}} & 0 \\ 0 & e^{-i\frac{\varphi}{2}} \end{bmatrix}. \quad (5)$$

The elements of the matrix O can be expanded in a Fourier series using³²

$$\begin{aligned} \cos \varphi &= J_0(\varphi_0) + 2J_2(\varphi_0) \cos(2\omega t) + \dots, \\ \sin \varphi &= 2J_1(\varphi_0) \sin(\omega t) + \dots, \end{aligned} \quad (6)$$

where $J_k(\varphi_0)$ is the Bessel function of harmonic order k . In this work, only a signal up to the second harmonic order was considered. After signal processing by the lock-in amplifier, it is possible to select only parts of the signal with a periodicity corresponding to the first or second harmonic of the modulating frequency. The Bessel functions for these harmonics are maximized when the phase φ_0 is set to $\varphi_0 = 1.885$ rad or $\varphi_0 = 3.054$ rad, respectively. However, to reduce any possible noise caused by the zeroth-order terms, it is often useful to set $\varphi_0 = 2.405$ rad instead so that $J_0(\varphi_0) = 0$. With the matrices presented above, we present in the following simulations for both the modulator-analyzer and modulator-PBS setups.

A. Modulator-analyzer (M-A) setup

For the modulator-analyzer (M-A) setup, the final polarization state is given by the product of the matrices corresponding to the relevant optical components as follows:

$$\begin{bmatrix} E_p \\ E_s \end{bmatrix}^f = AOSP. \quad (7)$$

The intensity of the signal detected is $I^{M-A} = |\mathbf{E}^f|^2 = |E_p|^2 + |E_s|^2$. It is the sum of the static signal I_0^{M-A} , the first harmonic signal $I_{1\omega}^{M-A}$, and the second harmonic signal $I_{2\omega}^{M-A}$,

$$\begin{aligned} I_0^{M-A} = J_0(\varphi_0) & [\cos^2 \beta \theta_p r_{pp}^2 + \sin^2 \beta \theta_s r_{ss}^2 \\ & + \frac{1}{2} \sin(2\beta) r_{pp} r_{ss} \cos(\delta_{ss} - \delta_{pp}) \\ & + \frac{1}{2} \sin(2\beta) r_{ps} r_{sp} \cos(\delta_{sp} - \delta_{ps})] \sin(2\alpha) \\ & + \sin(2\beta) r_{pp} r_{ps} \cos(\delta_{ps} - \delta_{pp}) \cos^2 \alpha \\ & + \sin(2\beta) r_{ss} r_{sp} \cos(\delta_{sp} - \delta_{ss}) \sin^2 \alpha \\ & + \cos^2 \beta r_{pp}^2 \cos^2 \alpha + \sin^2 \beta r_{ss}^2 \cos^2 \alpha \\ & + \sin^2 \beta r_{ss}^2 \sin^2 \alpha + \cos^2 \beta r_{sp}^2 \sin^2 \alpha, \end{aligned} \quad (8)$$

$$\begin{aligned} I_{1\omega}^{M-A} = J_1(\varphi_0) \sin(\omega t) & [2 \cos^2 \beta \varepsilon_p r_{pp}^2 - 2 \sin^2 \beta \varepsilon_s r_{ss}^2 \\ & - \sin(2\beta) \sin(\delta_{pp} - \delta_{ss}) r_{pp} r_{ss} \\ & - \sin(2\beta) \sin(\delta_{ps} - \delta_{sp}) r_{ps} r_{sp}] \sin(2\alpha), \end{aligned} \quad (9)$$

$$\begin{aligned} I_{2\omega}^{M-A} = J_2(\varphi_0) \cos(2\omega t) & [2 \cos^2 \beta \theta_p r_{pp}^2 + 2 \sin^2 \beta \theta_s r_{ss}^2 \\ & + \sin(2\beta) \sin(\delta_{pp} + \delta_{ss}) r_{pp} r_{ss} \\ & + \sin(2\beta) \sin(\delta_{ps} + \delta_{sp}) r_{ps} r_{sp}] \sin(2\alpha). \end{aligned} \quad (10)$$

As shown by Polisetty *et al.*,²⁴ the optimal configurations for the modulator-analyzer setup are $\beta = 90^\circ$ and $\alpha = 45^\circ$ or 135° . In these configurations, the detected intensity is

$$\begin{aligned} I^{M-A}(\beta = 90^\circ, \alpha = 45^\circ, 135^\circ) = & \frac{r_{ss}^2}{2} + \frac{r_{ps}^2}{2} \pm J_0(\varphi_0) \theta_s r_{ss}^2 \\ & \mp 2J_1(\varphi_0) \sin(\omega t) \varepsilon_s r_{ss}^2 \\ & \pm 2J_2(\varphi_0) \cos(2\omega t) \theta_s r_{ss}^2. \end{aligned} \quad (11)$$

Using the lock-in amplifier to read the first or second harmonic individually makes it possible to measure only the amplitude of one of the last two terms of Eq. (11), effectively isolating the Kerr ellipticity ε_s or rotation θ_s from other contributions. For example, in the present case, the intensity read in the first harmonic would be $2J_1(\varphi_0) \varepsilon_s r_{ss}^2$. To retrieve the Kerr ellipticity (or the Kerr rotation in the second harmonic), the signal must be normalized by a factor that contains r_{ss}^2 , which is usually constant for a given material and incidence angle. However, in the context of ultrafast magnetic dynamics, r_{ss}^2 can exhibit a time-dependent behavior that should be carefully characterized to allow the proper retrieval of the transient Kerr rotation or ellipticity.¹⁹ Fortunately, since the incident beam is s-polarized, r_{ss} simply corresponds to the reflectivity of the s-polarized component of the beam and can be easily measured. From Eqs. (8)–(10), we can further establish that the setup can be optimized for $\beta = 0^\circ$ (p-polarization). In this case, the detected intensity would be equivalent to Eq. (11) but with references to the Kerr rotation and ellipticity θ_p and ε_p instead of θ_s and ε_s .

B. Modulator-PBS (M-PBS) setup

The final polarization state for the modulator-PBS (M-PBS) setup is given by

$$\begin{bmatrix} E_p \\ E_s \end{bmatrix}^f = HOSP. \quad (12)$$

As mentioned above, there is no matrix to describe the polarization beam splitter. Instead, each component of the polarization (s and p) is independently detected. Then, these two signals are subtracted to one another and the difference is amplified by the balanced photodetectors. Therefore, the detected signal is proportional to $I^{M-PBS} = |E_p|^2 - |E_s|^2$. It corresponds to the sum of the static signal I_0^{M-PBS} , the first harmonic $I_{1\omega}^{M-PBS}$, and the second harmonic $I_{2\omega}^{M-PBS}$,

$$\begin{aligned} I_0^{M-PBS} = 2J_0(\varphi_0) & [\cos^2 \beta \theta_p r_{pp}^2 + \sin^2 \beta \theta_s r_{ss}^2 \\ & + \frac{1}{2} \sin(2\beta) r_{pp} r_{ss} \cos(\delta_{ss} - \delta_{pp}) \\ & + \frac{1}{2} \sin(2\beta) r_{ps} r_{sp} \cos(\delta_{sp} - \delta_{ps})] \sin(4\phi) \\ & + \sin(2\beta) r_{pp} r_{ps} \cos(\delta_{ps} - \delta_{pp}) \cos(4\phi) \\ & - \sin(2\beta) r_{ss} r_{sp} \cos(\delta_{sp} - \delta_{ss}) \cos(4\phi) \\ & + \cos^2 \beta r_{pp}^2 \cos(4\phi) + \sin^2 \beta r_{ss}^2 \cos(4\phi) \\ & - \sin^2 \beta r_{ss}^2 \cos(4\phi) - \cos^2 \beta r_{sp}^2 \cos(4\phi), \end{aligned} \quad (13)$$

$$\begin{aligned} I_{1\omega}^{M-PBS} = J_1(\varphi_0) \sin(\omega t) & [4 \cos^2 \beta \varepsilon_p r_{pp}^2 - 4 \sin^2 \beta \varepsilon_s r_{ss}^2 \\ & - 2 \sin(2\beta) \sin(\delta_{pp} - \delta_{ss}) r_{pp} r_{ss} \\ & - 2 \sin(2\beta) \sin(\delta_{ps} - \delta_{sp}) r_{ps} r_{sp}] \sin(4\phi), \end{aligned} \quad (14)$$

$$\begin{aligned} I_{2\omega}^{M-PBS} = J_2(\varphi_0) \cos(2\omega t) & [4 \cos^2 \beta \theta_p r_{pp}^2 + 4 \sin^2 \beta \theta_s r_{ss}^2 \\ & + 2 \sin(2\beta) \cos(\delta_{pp} - \delta_{ss}) r_{pp} r_{ss} \\ & + 2 \sin(2\beta) \cos(\delta_{ps} - \delta_{sp}) r_{ps} r_{sp}] \sin(4\phi). \end{aligned} \quad (15)$$

From the expressions for the first and second harmonics, it is obvious that the signal is maximized when $\phi = \{22.5^\circ, 67.5^\circ, 112.5^\circ, \dots\}$. Then, setting $\beta = 0^\circ$ or 90° cancels the terms that are not related to the Kerr rotation $\theta_{s,p}$ or ellipticity $\varepsilon_{s,p}$ while simultaneously maximizing the terms that are related to those quantities. Under such conditions, one example of the detected intensity is

$$I^{M-PBS}(\beta = 90^\circ, \phi = 22.5^\circ) = 2J_0(\varphi_0)\theta_s r_{ss}^2 - 4J_1(\varphi_0)\sin(\omega t)\varepsilon_s r_{ss}^2 + 4J_2(\varphi_0)\cos(2\omega t)\theta_s r_{ss}^2 \quad (16)$$

Once again, the lock-in amplifier allows selecting only the amplitude of the first (second) harmonic, which here corresponds to the second (third) term of the equation and allows us to isolate the Kerr ellipticity (rotation) from other contributions. As in the modulator-analyzer case, the result would be similar to different combinations of the optimized ϕ and β values. A different orientation of the half-waveplate may induce a sign change in one of the terms of the equation, and a switch from *s*-polarization to *p*-polarization would cause the intensity to be dependent on elements of the complex Kerr angle Θ_p instead of Θ_s , but no major change would occur in the form of the equation. It is interesting to note that this configuration is completely equivalent to the optimized modulator-analyzer setup while also being lossless. Indeed, in the case of the modulator-analyzer setup, the analyzer detects one component of the polarization in a basis that is rotated by 45° with respect to the plane of incidence. Equivalently, in the optimized configuration of the modulator-PBS setup, the half-waveplate is set to rotate an incident *s*- or *p*-polarization by 45° before both components of the polarization are detected in a basis that is aligned with the plane of incidence. While one component of the polarization of the beam would be rejected by the analyzer in the modulator-analyzer setup, here it is retained and measured. For this reason, Eq. (16) gives a detected intensity that is twice as strong as that given by Eq. (11). In addition, when $J_0(\varphi_0) = 0$, the static signal is canceled in the case of the modulator-PBS setup, which can contribute to improving the SNR.

C. Setups without the modulator and lock-in amplifier

The proposed setups described above can be used unchanged with MHz femtosecond pulse systems.³³ However, the relatively low pulse energy offered by these systems is insufficient to trigger ultrafast magnetic processes in magnetic thin films, making them unsuitable for time-resolved pump-probe investigations of these phenomena. Multi-kHz, millijoule, femtosecond laser systems are better adapted for this kind of study. Unfortunately, their rather low frequency makes the use of a modulator inconvenient, so time-resolved MOKE experiments based on these systems are routinely performed with the lock-in amplifier set at the laser pulse repetition frequency or half this frequency.³⁴ The response from the photodetector is typically faster than a microsecond, resulting in a low duty cycle (the period of the signal being on the order of hundreds of microseconds for a multi-kHz laser). For such a signal, the Fourier components are almost constant for tens to hundreds of harmonics, drastically reducing the amplitude measured by the lock-in amplifier

in one harmonic (for example, the fundamental) and consequently the SNR.

As an alternative, it is possible to use a setup without any modulator or chopper to improve the SNR.³⁵ Then, instead of going through the lock-in amplifier, either the detected signal can be electronically integrated over a defined time-period (boxcar detection)³⁶ or every pulse can be digitized. When removing the modulator, the detected intensity corresponds to I_0^{M-A} or I_0^{M-PBS} with $J_0(\varphi_0) = 1$. Therefore, the detected intensity in the optimal configuration calculated before for the PBS-based setup still delivers an isolated measurement of the Kerr rotation,

$$I^{PBS}(\beta = 90^\circ, \phi = 22.5^\circ) = 2\theta_s r_{ss}^2 \quad (17)$$

It should be noted that this PBS setup configuration does not allow for measurements of the Kerr ellipticity. However, if the half-waveplate is replaced by a quarter-waveplate oriented such that an *s*- or *p*-polarized incident beam becomes circularly polarized, the resulting signal is proportional to the Kerr ellipticity (see the [supplementary material](#)).

For the analyzer setup, by replacing $J_0(\varphi_0) = 1$ in Eq. (8), it becomes clear that no configuration allows for a direct measurement of the Kerr rotation. Indeed, there exists no combination of β and α for which the only non-zero term of the equation is proportional to the Kerr rotation or ellipticity. To overcome this, one strategy used in the literature is to slightly rotate the analyzer with respect to the crossed-polarizer case.²⁶ Then, considering that $r_{ps} \ll r_{ss}$, the signal can be approximated to

$$I^A(\beta = 90^\circ, \alpha \text{ small}) \approx 2\theta_s r_{ss}^2 \alpha + r_{ss}^2 \alpha^2 \quad (18)$$

for incident *s*-polarization, with an equivalent result for incident *p*-polarization. The Kerr rotation can be deduced if the nonmagnetic contribution r_{ss} is also measured. One more configuration of the analyzer-based setup deserves some attention: the simple case in which the analyzer is rotated by 90° with respect to the incident polarization. In this case, the measured intensity is, for incident *s*-polarization,

$$I^A(\beta = 90^\circ, \alpha = 0^\circ) = r_{ps}^2 \quad (19)$$

Then, it is not possible to directly determinate the Kerr rotation or ellipticity. Still, the measurement is of purely magneto-optical origin, making this simple configuration practical in certain contexts.

IV. EXPERIMENTAL RESULTS

A. Static experiment

Static measurements with varying magnetic field intensities were performed in order to compare the SNR of the modulator-analyzer and modulator-PBS setups. In both cases, the measurements were done on an iron sample with platinum capping deposited on a silicon substrate [Si/Ta 3/Pt 3/Fe 15/Pt 3 (nm)]. Since the orientation of magnetization for this sample is preferably in-plane, the setup geometry was chosen to be suitable for detecting the longitudinal MOKE [Fig. 1(a)]. The frequency of the PEM

was set to 50 kHz. A Wollaston prism was chosen as the polarizing beam splitter. The orientation of the prism was set so that both output beams have the same height. Since the beam height is kept constant throughout the setup, this ensures that the PBS adequately splits the *s*- and *p*-polarization components. The orientations of the polarizer and the half-waveplate were then defined from this basis. Balanced amplified photodetectors were used to further improve the SNR (PDB220A2/M, Thorlabs, Inc.). In order to make as few changes as possible between the measurements, the modulator-PBS setup was implemented and the modulator-analyzer setup was simulated by blocking one of the balanced photodetector's input while keeping the half-waveplate at 22.5° . Since the PBS separates *s*- and *p*-polarizations, this is equivalent to an analyzer set at 45° . The measured signal corresponds to the second harmonic of the modulating frequency detected by the lock-in amplifier, meaning that it is related to the Kerr rotation. The results are presented in Fig. 2.

As expected from the theoretical analysis, the signal obtained from the modulator-PBS setup is twice as strong as the one obtained from the modulator-analyzer setup. Consequently, the modulator-PBS setup also offers a much better SNR. Here, the SNR is defined as the ratio of the averaged intensity in the range of applied magnetic fields for which the magnetization of the sample is saturated to the standard deviation of the signal in the same range. The SNR for the modulator-analyzer setup is found to be 36.7, while it reaches 56.8 for the modulator-PBS setup, an improvement of >150%. More generally, the cancellation of common mode noise in balanced photodetectors leads to a greater SNR than the single photodetectors often used in analyzer-based MOKE setups, making PBS-based setups quite attractive.

As shown in Fig. 1(a), the longitudinal MOKE setup contains several reflections on mirrors. Mirrors, especially metallic ones, typically do not conserve the polarization state of the incident beam unless it is perfectly *s*- or *p*-polarized. This can have a considerable effect on the measured signal. For the optimized modulator-PBS and modulator-analyzer setups, the incident beam is *s*- or *p*-polarized, so the effect of the mirrors up to the sample position can be neglected. However, between the sample and the detection scheme, there are three reflections on protected silver

mirrors (Thorlabs, Inc.) that should be taken into account. By adding a matrix representing a mirror to the calculations presented in Sec. III, it can be shown that the signals of the Kerr rotation and ellipticity become mixed (see the [supplementary material](#)). For a mirror with a complex reflectivity $r_{m,p}e^{i\xi_p}$ for the *p*-polarization and $r_{m,s}e^{i\xi_s}$ for the *s*-polarization, the measured signal of the optimized modulator-PBS becomes

$$\begin{aligned} I^{M-PBS}(\beta = 90^\circ, \phi = 22.5^\circ) &= 2J_0(\varphi_0)[\theta_s \cos(\Delta\xi) - \varepsilon_s \sin(\Delta\xi)]r_{m,p}r_{m,s}r_{ss}^2 \\ &\quad - 4J_1(\varphi_0)\sin(\omega t)[\varepsilon_s \cos(\Delta\xi) + \theta_s \sin(\Delta\xi)]r_{m,p}r_{m,s}r_{ss}^2 \\ &\quad + 4J_2(\varphi_0)\cos(2\omega t)[\theta_s \cos(\Delta\xi) - \varepsilon_s \sin(\Delta\xi)]r_{m,p}r_{m,s}r_{ss}^2. \end{aligned} \quad (20)$$

For protected silver mirrors near 45° incidence, the phase difference $\Delta\xi = \xi_p - \xi_s$ is significant. Consequently, a strong MOKE signal can still be obtained, but the Kerr rotation and ellipticity cannot be independently retrieved. This implies that in our experiment, we are only sensitive to a relative change in the magnetization and not to the absolute Kerr rotation and ellipticity.

However, by carefully choosing the mirrors and designing the setup as to minimize reflections, the phase difference $\Delta\xi$ can become negligible, and such a MOKE setup can be used to retrieve absolute values of the Kerr rotation and ellipticity. To do so, it is necessary to calibrate the signal to extract the amplifying factor of the detectors. As described in the study by Buchmeier *et al.*,³⁷ this can be achieved by using a non-magnetic sample with a known refractive index for the calibration.

B. Time-resolved experiment

As an example of time-resolved measurements, we have characterized the ultrafast demagnetization of a Co/Pt multilayer sample excited by a femtosecond laser pulse. This phenomenon, discovered in 1996 by Beaurepaire *et al.*,¹⁰ occurs within a few hundred femtoseconds after the excitation of a ferromagnetic material by a laser pulse.³⁸ Despite having been studied for many years, the underlying mechanisms of ultrafast demagnetization are still the subject of intense research.³⁹

A sketch of the experimental pump-probe setup is shown in Fig. 3. The experiment was performed in the Corail room of the Laboratoire d'Optique Appliquée. A titanium-sapphire laser system delivers femtosecond pulses with an energy of 2 mJ at 800 nm. About 1% of this energy is used for this experiment. Because the beam is transmitted through thick optical elements that stretch the pulse before reaching the MOKE setup, the pulse duration is ~ 100 fs long. The beam is frequency-doubled, and the fundamental and second-harmonic beams are used as the pump and probe, respectively. A delay line is placed in the pump beam path, making it possible to record the Kerr rotation as a function of time. To avoid issues related to modulation and signal recovery at the low repetition rate of the laser system (5 kHz), the PBS setup is used without the modulator and the lock-in amplifier. The sample is magnetized out-of-plane by an electromagnet, which provides a weak magnetic field (<200 mT). Because this electromagnet can only be used to generate a magnetic field normal to the sample surface, a typical multilayer sample (Si/Ta

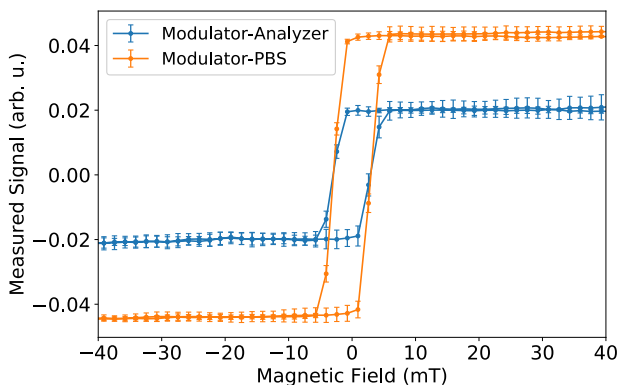


FIG. 2. Second harmonic of longitudinal MOKE measurements made with the modulator-analyzer (blue) and modulator-PBS (orange) setups for a Si/Ta 3/Pt 3/Fe 15/Pt 3 (nm) sample. The error bars correspond to the standard deviation of a set of four measurements.

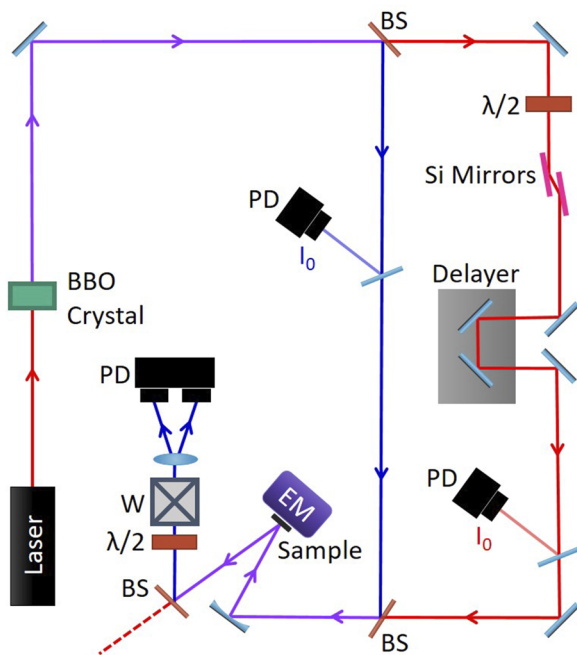


FIG. 3. Experimental time-resolved MOKE setup. The laser is a titanium-sapphire system with an output wavelength of 800 nm. The beam is frequency-doubled in a BBO crystal. Dichroic beam splitters are used to separate and recombine the pump (red) and probe (blue) beams. The fluence of the pump beam on the sample is controlled by a half-waveplate coupled with a pair of Si mirrors acting as polarizers. Photodetectors are placed along the paths of the beams to keep track of their intensities.

3/Pt5/[Co 0.6/Pt 0.8]×20/Al 3 (nm)) with high out-of-plane magnetic anisotropy was chosen along with a polar MOKE geometry.⁴⁰ For each laser shot, a digitizer (WaveCatcher) is used to record at least four waveforms: the three outputs of the balanced photodetectors, namely, both photodiodes and their amplified difference (RF signal), and the intensity of the pump pulse.⁴¹ An additional photodetector placed on the probe path can also be used to measure the probe intensity. These measurements allow us to normalize the Kerr signal by the probe intensity to compensate for fluctuations of the laser power and could be used to sort the data by pump fluence if the variations in the pump intensity were sufficiently large. Each detected signal is digitized. This approach was favored in this work as it has the advantage that the waveform is recorded on a shot by shot basis, allowing for more complex sorting and integration of the data.

Figure 4(a) shows two RF signal waveforms recorded for a single shot at positive (orange line) and negative (blue line) delays. To obtain a full demagnetization curve, we record such waveforms for each laser pulse while slowly and continuously varying the position of the delay stage. The position of the stage is recorded with the same frequency as the repetition rate of the laser, allowing us to retrieve the actual delay position for each laser pulse. We perform such a delay scan for each of the opposite magnetization directions. Then, we extract the integral of the waveforms normalized by the incoming probe intensity as a function of delay [variable named $I^{+/-}(t)$ in the

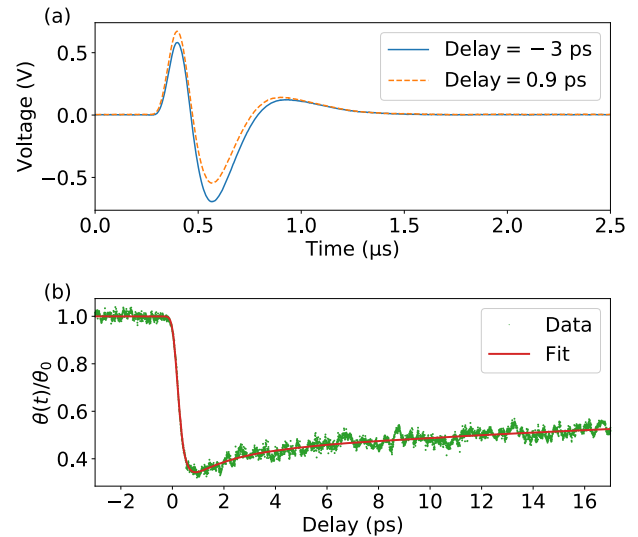


FIG. 4. (a) RF output waveforms of the balanced photodetector recorded before (blue solid line) and after (orange dotted line) excitation by the optical pump pulse. The difference between the two waveforms is a consequence of the demagnetization of the sample. (b) Normalized Kerr rotation as a function of time delay for the same sample (green dots). The solid red line shows a bi-exponential fit of the data.

following]. By taking the difference between the recorded intensities with the two magnetization directions, we can retrieve the amplitude of the change in the Kerr rotation,

$$\frac{\theta(t)}{\theta_0} = \frac{I^+(t) - I^-(t)}{I^+(t < 0) - I^-(t < 0)}. \quad (21)$$

This time trace is shown in Fig. 4(b). To produce this curve, 200 000 shots were recorded (100 000 for each magnetization direction), within a total of only 40 s. By fitting the curve with a typical expression used for transient demagnetization,⁴² we find a demagnetization time of 187 ± 9 fs, in agreement with previous studies on this type of sample.⁴³ It should be noted that studies are ongoing to define whether Kerr rotation measurements constitute a pure representation of the ultrafast magnetization dynamics.^{18,19}

V. CONCLUSION

The Jones formalism is used to derive mathematical expressions to analyze the signal measured from different MOKE setups and define the optimal orientation of their optical components. When a photoelastic modulator and a lock-in amplifier are used, it is found that the Kerr ellipticity and rotation can be measured directly by looking at the first or second harmonic of the modulating frequency of the signal, respectively, in both analyzer-based and polarizing beam splitter-based detection schemes. Additionally, we demonstrate, through the theoretical analysis and experimental results, that the polarizing beam splitter-based setup improves the intensity of the signal by a factor of two. As a result, and because the use of balanced photodetectors helps reduce the noise, the signal-to-noise ratio is demonstrated to increase by at least 150% compared to the analyzer-based detection scheme. Furthermore, it is shown that the

polarizing beam splitter-based setup is also suitable for measuring the Kerr rotation without the use of a modulator and lock-in amplifier, which can be advantageous for pulsed laser sources with low repetition rates. In contrast, equations show that the Kerr rotation cannot be isolated with an analyzer-based setup. In this case, the only configuration that allows for purely magneto-optical measurements consists of placing the optical axis of the analyzer at 90° with respect to the incident polarization. To assess the applicability of the optimal setup configuration, time-resolved measurements of laser-induced ultrafast demagnetization from a kHz laser system are recorded. The high signal-to-noise ratio offered by the balanced photodetectors allows for sensitive, single-shot measurements of the Kerr rotation for each delay, leading to a fast acquisition time. Importantly, we demonstrate that reflections on mirrors can be detrimental to the independent measurement of Kerr rotation and ellipticity and should be carefully considered in the design of MOKE setups. This illustrates how the general expressions presented in this work can serve as a valuable tool to guide the design of future MOKE setups by revealing the optimal experimental parameters for the measurement of any component of the complex Kerr angles.

SUPPLEMENTARY MATERIAL

See the [supplementary material](#) for a detailed example of the matrix calculation for the optimized modulator-analyzer setup, the analytic description of the PBS setup with the half-waveplate replaced by a quarter-waveplate for Kerr ellipticity measurements, and also a thorough description of the effect of mirror reflections on the measured MOKE signal.

ACKNOWLEDGMENTS

This work was supported by the Agence nationale de la recherche (ANR) (Grant No. ANR-15-CE24-0009-03), the Investissements d'Avenir of LabEx PALM (Grant No. ANR-10-LABX-0039-PALM), CNRS-MOMENTUM, CNRS-IEA STERIOD, and the Natural Sciences and Engineering Research Council of Canada (NSERC).

AUTHOR DECLARATIONS

Conflict of Interest

The authors have no conflicts to disclose.

Author Contributions

Katherine Légaré: Formal analysis (lead); Writing – original draft (lead); Writing – review & editing (lead). **Valentin Chardonnet:** Data curation (supporting). **Ivette Bermúdez Macías:** Data curation (equal). **Marcel Hennes:** Conceptualization (equal); Data curation (equal). **Renaud Delaunay:** Data curation (equal); Resources (equal). **Philippe Lassonde:** Writing – review & editing (equal). **François Légaré:** Funding acquisition (equal). **Guillaume Lambert:** Data curation (equal); Resources (equal); Writing – review & editing (equal). **Emmanuelle Jal:** Conceptualization (equal); Data curation (equal); Funding acquisition (equal); Methodology (equal);

Supervision (equal); Writing – original draft (supporting); Writing – review & editing (equal). **Boris Vodungbo:** Conceptualization (equal); Data curation (equal); Funding acquisition (equal); Methodology (equal); Supervision (equal); Writing – original draft (supporting); Writing – review & editing (equal).

DATA AVAILABILITY

The data that support the findings of this study are available from the corresponding authors upon reasonable request.

REFERENCES

- ¹J. Kerr, *London, Edinburgh Dublin Philos. Mag. J. Sci.* **3**, 321 (1877).
- ²R. Schäfer and J. McCord, in *Magnetic Measurement Techniques for Materials Characterization*, edited by V. Franco and B. Dodrill (Springer International Publishing, Cham, 2021), pp. 171–229.
- ³E. R. Moog and S. D. Bader, *Superlattices Microstruct.* **1**, 543 (1985).
- ⁴M. R. Pufall, C. Platt, and A. Berger, *J. Appl. Phys.* **85**, 4818 (1999).
- ⁵S. Maat, L. Shen, C. Hou, H. Fujiwara, and G. J. Mankey, *J. Appl. Phys.* **85**, 1658 (1999).
- ⁶Y. Guan, T. Koyama, and D. Chiba, *AIP Adv.* **7**, 085123 (2017).
- ⁷A. Neudert, J. McCord, R. Schäfer, and L. Schultz, *J. Appl. Phys.* **97**, 10E701 (2005).
- ⁸D. Jenkins, W. Clegg, J. Windmill, S. Edmund, P. Davey, D. Newman, C. D. Wright, M. Loze, M. Armand, R. Atkinson, B. Hendren, and P. Nutter, *Microsyst. Technol.* **10**, 66 (2003).
- ⁹A. Hirohata, K. Yamada, Y. Nakatani, I.-L. Prejbeanu, B. Diény, P. Pirro, and B. Hillebrands, *J. Magn. Magn. Mater.* **509**, 166711 (2020).
- ¹⁰E. Beaurepaire, J.-C. Merle, A. Daunois, and J.-Y. Bigot, *Phys. Rev. Lett.* **76**, 4250 (1996).
- ¹¹C. D. Stanciu, F. Hansteen, A. V. Kimel, A. Kirilyuk, A. Tsukamoto, A. Itoh, and Th. Rasing, *Phys. Rev. Lett.* **99**, 047601 (2007).
- ¹²T. Haider, *Int. J. Electromagn. Appl.* **7**, 17 (2017).
- ¹³S.-K. Kim, J.-W. Lee, S.-C. Shin, and K. Y. Kim, *J. Appl. Phys.* **91**, 3099 (2002).
- ¹⁴L. Lounis, M. Eddrief, M. Sacchi, and F. Vidal, *Appl. Phys. Lett.* **111**, 232403 (2017).
- ¹⁵G. P. Zhang, W. Hübner, G. Lefkidis, Y. Bai, and T. F. George, *Nat. Phys.* **5**, 499 (2009).
- ¹⁶P. M. Oppeneer and A. Liebsch, *J. Phys.: Condens. Matter* **16**, 5519 (2004).
- ¹⁷B. Koopmans, M. van Kampen, J. T. Kohlhepp, and W. J. M. de Jonge, *Phys. Rev. Lett.* **85**, 844 (2000).
- ¹⁸I. Razdolski, A. Alekhin, U. Martens, D. Büstel, D. Diesing, M. Münzenberg, U. Bovensiepen, and A. Melnikov, *J. Phys.: Condens. Matter* **29**, 174002 (2017).
- ¹⁹E. Carpane, F. Boschini, H. Hedayat, C. Piovera, C. Dallera, E. Puppini, M. Mansurova, M. Münzenberg, X. Zhang, and A. Gupta, *Phys. Rev. B* **87**, 174437 (2013).
- ²⁰J. Wiczorek, A. Eschenlohr, B. Weidtmann, M. Rösner, N. Bergeard, A. Tarasevitch, T. O. Wehling, and U. Bovensiepen, *Phys. Rev. B* **92**, 174410 (2015).
- ²¹R. P. Hunt, *J. Appl. Phys.* **38**, 1652 (1967).
- ²²C.-Y. You and S.-C. Shin, *J. Appl. Phys.* **84**, 541 (1998).
- ²³J. Zak, E. R. Moog, C. Liu, and S. D. Bader, *J. Magn. Magn. Mater.* **89**, 107 (1990).
- ²⁴S. Polisetty, J. Scheffler, S. Sahoo, Y. Wang, T. Mukherjee, X. He, and Ch. Binck, *Rev. Sci. Instrum.* **79**, 055107 (2008).
- ²⁵V. Usov, S. Murphy, L. Seravalli, and I. V. Shvets, *Rev. Sci. Instrum.* **76**, 046102 (2005).
- ²⁶Z. Q. Qiu and S. D. Bader, *Rev. Sci. Instrum.* **71**, 1243 (2000).
- ²⁷A. Berger and M. R. Pufall, *Appl. Phys. Lett.* **71**, 965 (1997).
- ²⁸W. W. Clegg, N. A. E. Heyes, E. W. Hill, and C. D. Wright, *J. Magn. Magn. Mater.* **95**, 49 (1991).
- ²⁹M. R. Freeman and J. F. Smyth, *J. Appl. Phys.* **79**, 5898 (1996).
- ³⁰K. Sato, *Jpn. J. Appl. Phys.* **20**, 2403 (1981).

- ³¹P. Kasiraj, R. Shelby, J. Best, and D. Horne, *IEEE Trans. Magn.* **22**, 837 (1986).
- ³²I. S. Gradshteyn and I. M. Ryzhik, *Table of Integrals, Series, and Products*, 7th ed. (Academic Press, 2007).
- ³³T. Henn, T. Kiessling, W. Ossau, L. W. Molenkamp, K. Biermann, and P. V. Santos, *Rev. Sci. Instrum.* **84**, 123903 (2013).
- ³⁴E. Carpena, E. Mancini, C. Dallera, M. Brenna, E. Puppini, and S. De Silvestri, *Phys. Rev. B* **78**, 174422 (2008).
- ³⁵A. Weber, F. Pressacco, S. Günther, E. Mancini, P. M. Oppeneer, and C. H. Back, *Phys. Rev. B* **84**, 132412 (2011).
- ³⁶J. Wang, G. A. Khodaparast, J. Kono, T. Slupinski, A. Oiwa, and H. Munekata, in *Proceedings of the IEEE Lester Eastman Conference on High Performance Devices* (IEEE, 2002), pp. 307–314.
- ³⁷M. Buchmeier, R. Schreiber, D. E. Bürgler, and C. M. Schneider, *Phys. Rev. B* **79**, 064402 (2009).
- ³⁸B. Koopmans, G. Malinowski, F. Dalla Longa, D. Steiauf, M. Fähnle, T. Roth, M. Cinchetti, and M. Aeschlimann, *Nat. Mater.* **9**, 259 (2010).
- ³⁹M. Fähnle, M. Haag, C. Illg, B. Mueller, W. Weng, T. Tsatsoulis, H. Huang, J. Briones, N. Teeny, L. Zhang, and T. Kuhn, *Am. J. Mod. Phys.* **7**, 68 (2018).
- ⁴⁰O. Hellwig, A. Berger, J. B. Kortright, and E. E. Fullerton, *J. Magn. Magn. Mater.* **319**, 13 (2007).
- ⁴¹D. Breton, E. Delagnes, J. Maalmi, and P. Rusquart, in *2014 19th IEEE-NPSS Real Time Conference* (IEEE, 2014), pp. 1–8.
- ⁴²M. Hennes, A. Merhe, X. Liu, D. Weder, C. v. K. Schmising, M. Schneider, C. M. Günther, B. Mahieu, G. Malinowski, M. Hehn, D. Lacour, F. Capotondi, E. Pedersoli, I. P. Nikolov, V. Chardonnet, E. Jal, J. Lüning, and B. Vodungbo, *Phys. Rev. B* **102**, 174437 (2020).
- ⁴³N. Moisan, G. Malinowski, J. Mauchain, M. Hehn, B. Vodungbo, J. Lüning, S. Mangin, E. E. Fullerton, and A. Thiaville, *Sci. Rep.* **4**, 4658 (2014).